SCIENTIFIC REPORTS

OPEN

SUBJECT AREAS:
QUANTUM DOTS
INFRARED SPECTROSCOPY
ELECTRONIC PROPERTIES AND MATERIALS
NANOSCIENCE AND TECHNOLOGY

Received
29 May 2013

Accepted
30 May 2013

Published
18 June 2013

Correspondence and requests for materials should be addressed to V.I.K. (klimov@lanl.gov)

* These authors contributed equally to this work.

Heavily doped *n*-type PbSe and PbS nanocrystals using ground-state charge transfer from cobaltocene

Weon-kyu Koh*, Alexey Y. Koposov*, John T. Stewart, Bhola N. Pal, Istvan Robel, Jeffrey M. Pietryga & Victor I. Klimov

Center for Advanced Solar Photophysics, Los Alamos National Laboratory, New Mexico 87545, United States.

Colloidal nanocrystals (NCs) of lead chalcogenides are a promising class of tunable infrared materials for applications in devices such as photodetectors and solar cells. Such devices typically employ electronic materials in which charge carrier concentrations are manipulated through "doping;" however, persistent electronic doping of these NCs remains a challenge. Here, we demonstrate that heavily doped *n*-type PbSe and PbS NCs can be realized utilizing ground-state electron transfer from cobaltocene. This allows injecting up to eight electrons per NC into the band-edge state and maintaining the doping level for at least a month at room temperature. Doping is confirmed by inter- and intra-band optical absorption, as well as by carrier dynamics. Finally, FET measurements of doped NC films and the demonstration of a *p-n* diode provide additional evidence that the developed doping procedure allows for persistent incorporation of electrons into the quantum-confined NC states.

Electronic devices often achieve maximum performance by using electronic doping of their constituent electronic materials to exert control over charge carrier behavior. A powerful example is the use of the internal fields within the *p-n* junction of many common types of photovoltaic solar cells to achieve efficient carrier separation. Colloidal semiconductor nanocrystals (NCs) are the subject of vigorous and widespread investigation for use in low-cost, efficient electronic devices[1–3]. Increasingly, focus is shifting to realizing and exploiting electronic doping in these materials, particularly in infrared NCs, like the lead chalcogenides, which are of direct importance for solar cells. Reported approaches to NC-doping have utilized incorporation of metal ions[4], chemical treatments[5,6], or electrochemical charge injection[7], but "heavy doping" of lead chalcogenide NCs (persistent introduction of multiple charges into the quantum-confined band-edge states) still represents a significant challenge.

Apparent *n*- and *p*-type behaviors have been imparted via surface treatment of PbS and PbSe NCs with chemical species such as hydrazine or ethanedithiol (EDT)[1,8], and effective carrier densities within *p*-type films of EDT-treated NCs can be further manipulated by charge injection from chemical redox agents[6]. However, studies of field-effect transistors (FETs) based on EDT-treated PbS NCs indicate that these procedures introduce charges not into the NC quantum-confined band-edge states, but rather into surface trap sites within the NC assembly[9]. While this approach can improve dark conductivity, it does not allow for precise control of the doping level, and the resulting emergence of a band of mid-gap states causes unwanted phenomena such as fast trapping of minority carriers and pinning of the open circuit voltage in photovoltaic cells[9]. Likewise, introduction of metal-ion impurity "dopants" into InAs NCs, another infrared-active material, has also resulted in *n*- or *p*-type conductivity based transport of carriers through trap states[10], which at extreme doping levels may form distinct impurity-based sub-bands[4]. On the other hand, adding carriers directly into the quantum-confined band-edge NC states offers better control of device performance, as these states reside at predictable, size-tunable energies, and exhibit well-understood degeneracies and recombination dynamics.

Injection of electrons into band-edge NC states has been accomplished in relatively wide-gap materials, such as CdSe or ZnO NCs[5], by reaction with strong reducing agents such as sodium biphenyl. However, attempts to reproduce these effects in lead chalcogenide-based materials are frustrated by severe degradation of the NCs, as these materials are considerably less chemically robust toward redox chemistry[11], ion-exchange[12], and more complex processes associated with disruption of the ligand shell[13]. An alternative approach suitable for PbSe is to inject charges into NCs deposited on an electrode within an electrochemical cell[7]. This method offers excellent

control over doping levels, and thus is very useful for, *e.g.*, spectroscopic studies in a laboratory setting; however, the necessity of maintaining an additional externally applied bias to preserve the NC-doping is impractical in a functional device. Thus, there is still a need for a simple, non-destructive method for persistent addition of charge carriers into the band-edge states of lead chalcogenide NCs.

Here, we report the chemical doping of these materials with molecules of cobaltocene, a mild, non-polar-soluble reducing agent. Typically, *n*-type PbSe and PbS NCs are prepared by simple mixing of NC dispersions with various concentrations of cobaltocene in toluene (see Methods for details). Ground-state electron transfer from cobaltocene to quantized NC band-edge states is confirmed using optical absorption and photoluminescence (PL) spectroscopy, as well as transient absorption (TA) spectroscopy. As true electronic doping of the NCs can be achieved by this approach, we also study the effect of incorporated charges into the quantum-confined states within the NC core by FETs and *p-n* junction diode measurements.

Results

The effect of doping on inter-band and intra-band optical absorption. The reduction potential of cobaltocene is −0.69 V vs. SHE[14] which lies above the conduction band edge of both bulk PbSe (0.2 V vs. SHE) and PbS (0.1 V vs. SHE)[15]. Importantly, the driving force for electron transfer in NCs is modified by the effects of quantum confinement: as the conduction band edge of the NCs shifts up in energy with decreasing NC dimensions (Fig. 1a), the driving force decreases, and the process becomes unfavorable at very small sizes. On the basis of size-dependent band energies from a recent report by Jasieniak, *et al.*[16], we should expect that electron transfer from cobaltocene to the PbSe and PbS NCs is energetically favorable for particle sizes greater than ~3.2 nm and ~4.2 nm, respectively.

Once electrons are transferred to the $1S_e$ conduction band state, the amplitude of the 1S peak is expected to be reduced (bleached; Fig. 1b) due to Pauli blocking, by an amount ($\Delta\alpha_1$) that scales directly with the number of electrons injected into the NC (N_e). In the case of PbSe and PbS NCs with an 8-fold degenerate $1S_e$ state[17], this scaling can be described by $|\Delta\alpha_1|/\alpha_{01} = |\alpha_1 - \alpha_{01}|/\alpha_{01} = N_e/8$[18], where α_{01} and α_1 are the amplitudes of the 1S absorption peak in the untreated and treated samples, respectively.

Indeed, when we mix cobaltocene (~5 mM in toluene) with PbSe NCs (1.5 μM in toluene), we observe a dramatic reduction of the 1S peak amplitude (Fig. 1c), similar to that observed in previous electrochemical doping studies[7] and in contrast to previously reported ligand-exchange doping methods that do not result in 1S bleaching[6,9,19]. The effect is most pronounced in the largest NCs (7.9 nm diameter with band gap E_g = 0.60 eV) in which the 1S feature is completely bleached, indicating that the NC contains at least *eight* electrons. This is an extremely high doping level by bulk semiconductor standards: in terms of carrier concentration, it translates into an electron density of more than 10^{19} cm^{-3}. The band-edge bleaching decreases in smaller NC sizes until it becomes essentially unnoticeable in the smallest particles (Fig. 1c; bottom spectrum). This trend indicates a reduction in the doping density, and confirms the expected drop in the charge-transfer efficiency due to reduction in the driving force in smaller NCs (see Fig. 1a, circles); very similar trends are also observed in PbS NCs (Fig. 1a, squares; Fig. 1d).

By using different concentrations of cobaltocene, we can control the level of doping. As illustrated in Fig. 2a, the increase in the amount of cobaltocene from 20 μM to 5 mM for the same concentration of the PbSe NCs (7.9 nm diameter), the amplitude of the 1S peak at 0.60 eV (Fig. 2a) decreases monotonically. Interestingly, we also observe simultaneous partial bleaching of the second absorption peak, while the third absorption feature remains virtually unchanged. To analyze these results in quantitative terms, we fit the band-edge absorption to the sum of three Gaussian peaks (Fig. 2b). A plot of the amplitudes of the peaks (α_1, α_2, and α_3) as a function of cobaltocene concentration (Fig. 2c) reveals clear correlations in the bleaching of the first and the second absorption features. Specifically, if we plot the normalized bleach amplitude of the second peak $\Delta\alpha_2/\alpha_{02}$ vs. $\Delta\alpha_1/\alpha_{01}$, we see that they are related by a factor of ~0.5 (inset of Fig. 2c).

This observation can be explained if we assume that the second absorption feature is due to the two nominally parity forbidden transitions $1P_h - 1S_e$ and $1S_h - 1P_e$. (It has been suggested that parity conservation in lead chalcogenide NCs can be broken due to internal electric field and/or asymmetry in the distribution of atoms with

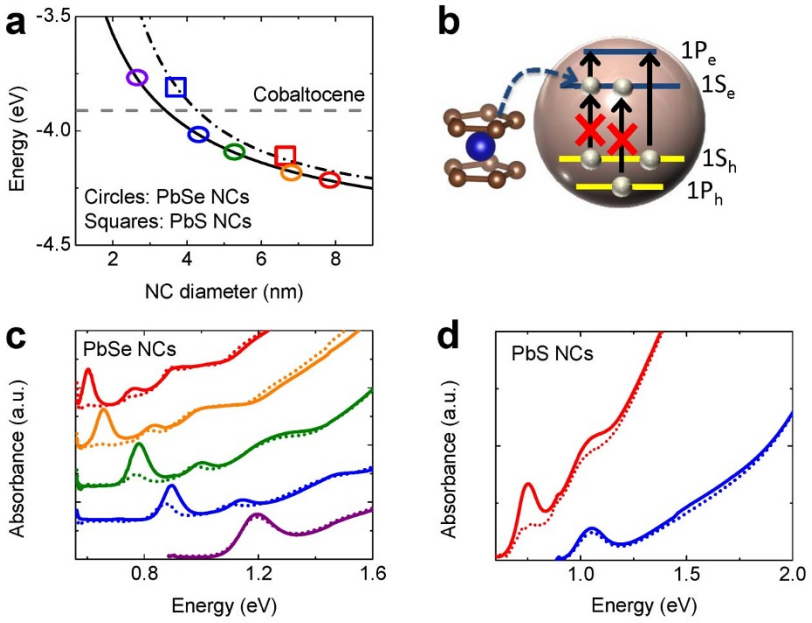

Figure 1 | Cobaltocene doping of PbSe and PbS NC solutions. (a) The redox potential of cobaltocene (dashed gray line) in comparison to the conduction band states in PbSe (solid black line) and PbS (dashed-dotted black line) NCs. Symbols correspond to samples from the present study. (b) The effect of electron injection from cobaltocene on optical absorption of a NC. NC-size dependent absorption spectra of PbSe (c) and PbS (d) NCs before (solid lines) and after (dashed lines) treatment with cobaltocene; color coding matches that in panel a.

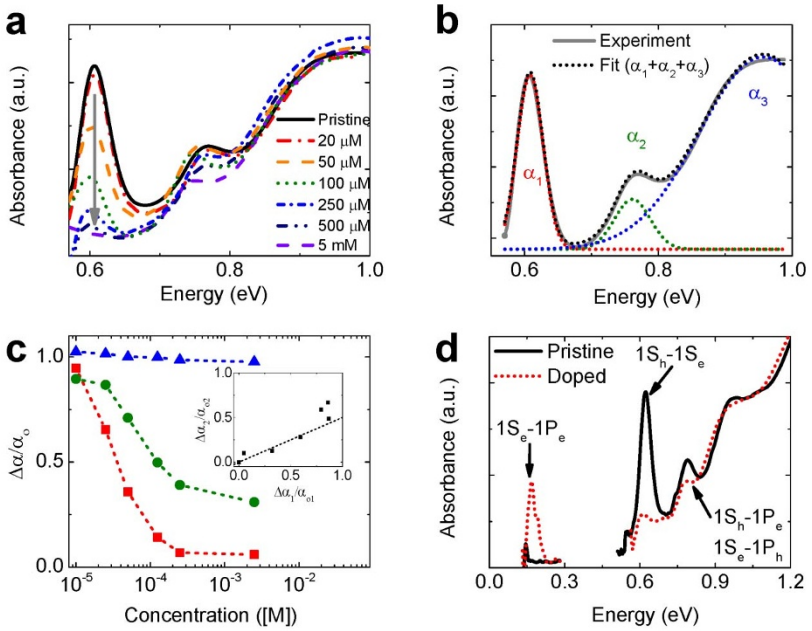

Figure 2 | Effect of treatment with cobaltocene on inter-band and intra-band absorption spectra of PbSe NCs. (a) Absorption spectra of 7.9 nm diameter PbSe NCs as a function of cobaltocene concentration. (b) Fitting of the absorption spectrum of pristine PbSe NCs to the sum of the three Gaussian bands (dashed black line) that describe the 1st (α_1, dash red line), 2nd (α_2, dash green line), and 3rd (α_3, dash blue line) inter-band transitions. (c) Normalized absorption intensity $\Delta\alpha_i/\alpha_i$ (i = 1, 2, 3) in each transition (1st: red squares; 2nd: green circles, 3rd: blue triangles) for treated PbSe NCs as a function of the concentration of cobaltocene. Inset: Correlation of $\Delta\alpha_1/\alpha_{o1}$ and $\Delta\alpha_2/\alpha_{o2}$. (d) Pristine (solid black line) and cobaltocene-treated (dash red line) PbSe NCs.

regard to the NC center, allowing these forbidden transitions[20].) Because of mirror symmetric valence and conduction bands in PbSe, these transitions have the same energy and strength, and should overlap in the absorption spectrum; hence, α_2 can be presented as $\alpha_{02} = \alpha_0(1P_h,1S_e) + \alpha_0(1S_h,1P_e) = 2\alpha_0(1P_h,1S_e)$. If electrons are introduced into the $1S_e$ state, the contribution to α_2 from the $1S_h - 1P_e$ transition is unchanged, while the contribution due to the $1P_h - 1S_e$ transition is bleached according to $\Delta\alpha(1P_h,1S_e) = (N_e/8)\alpha_0(1P_h,1S_e)$[18]; see Fig. 1b. As a result, $\Delta\alpha_2/\alpha_{02} = N_e/16$, that is, $\Delta\alpha_2/\alpha_{02} = 0.5\Delta\alpha_1/\alpha_{01}$. This is exactly what is seen experimentally.

Along with bleaching of inter-band absorption peaks, doping is expected to activate a new absorption feature in the mid-infrared due to the allowed intra-band transition of the injected electrons from the $1S_e$ to the $1P_e$ level[5,7] (Fig. 1b). If, as stated above, the second peak in inter-band absorption is due to the $1S_{h,e}$ -$1P_{e,h}$ transition, its separation from the 1S peak provides a measure of the energy of the intra-band $1S_e$ -$1P_e$ transition, which for 7.9 nm PbSe NCs is 165 meV (Fig. 2d, black solid line). Indeed, along with 1S bleaching, cobaltocene-treatment of these NCs produces a new mid-infrared feature located exactly at 165 meV (Fig. 2d, red dashed line), which cannot be attributed to absorption by cobaltocenium counterion (Supplemental Fig. S1).

The effect of doping on photoluminescence. Doping of quantum-confined band-edge states should also have a dramatic effect on the dynamics of photogenerated charges in NCs, and thus on PL quantum yield. On the basis of statistical considerations[21,22], the radiative lifetime of an exciton in the presence of N_e extra charges ($\tau_{r,XNe}$) is shorter than that of a neutral exciton ($\tau_{r,X}$, typically 100s of ns[23]) by a factor of (N_e + 1). In reality, if even one additional electron is introduced into the NC, the measured lifetime of the singly-charged exciton ($\tau_{A,X1-}$) – a state known as a negative trion - is characterized by sub-ns time constants[22]. This is due to activation of efficient, nonradiative Auger decay, whereby the recombination energy of an electron-hole pair is transferred to the extra carrier within the NC. The Auger decay lifetime (τ_A) scales inversely with the number of available recombination pathways[24]. In the case of a single exciton generated in the NC doped with N_e electrons, $\tau_{A,XNe}$ can be expressed in terms of the well-established biexciton Auger lifetime ($\tau_{A,XX}$) as $\tau_{A,XNe} = (8\tau_{A,XX})/[N_e(N_e + 1)]$.

The effect of the combined contributions of radiative and Auger recombination to overall PL efficiency within doped NCs can be described in terms of the PL suppression factor, β. For an individual NC with N_e extra electrons, $\beta = Q_{Ne}/Q_0 = (8/N_e)(\tau_{A,XX}/\tau_X)$, where $Q_0 = \tau_X/\tau_{r,X}$ is the neutral exciton PL quantum yield (τ_{rX} is its total lifetime), and $Q_{Ne} = \tau_{A,XNe}(N_e + 1)/\tau_{r,X}$ is the charged exciton PL quantum yield. Based on these expressions, a single excess charge is expected to suppress PL by a factor of at least 1000, due to the dramatic difference between the single-exciton radiative lifetime and biexciton Auger lifetime. This is in sharp contrast to the effect on the band-edge absorption feature, which is only bleached by a factor of $N_e/8$ (*i.e.*, 12.5% for a single excess electron).

We use the above considerations to model the effect of injected electrons on PL assuming that extra charges are distributed across the NC sample according to Poisson statistics: $p_i = (\langle N_e\rangle^i/i!)\exp(-\langle N_e\rangle)$, where p_i is the probability of having i electrons in a given NC if the average number of injected electrons is $\langle N_e\rangle$. In this case, the ensemble-averaged PL suppression factor can be presented as $\langle\beta\rangle = p_0 + (8\tau_{A,XX}/\tau_X)\sum_{i=1}^{\infty} p_i i^{-1}$. As $\tau_{A,XX}/\tau_X \ll 1$, the ensemble PL quenching factor can be approximated by the fraction of uncharged NCs, that is, $\langle\beta\rangle \approx p_0$. In Fig. 3a, we apply this approximation to model the PL quantum yield of the sample with E_g = 0.60 eV. Using $\langle N_e\rangle$ from the bleach of the 1S absorption peak, we obtain excellent agreement with the measured data (inset of Fig. 3a; compare symbols and solid line) without any adjustable parameters. This correlation holds true for all NC sizes, which is to say that smaller NCs that exhibit less 1S bleach also show less PL suppression (Supplemental Fig. S2).

The effect of doping on carrier dynamics. Next, we directly monitor photoexcited NC dynamics as a function of doping level using TA experiment[25]. We first measure the pristine sample and find $\tau_{A,XX}$ to

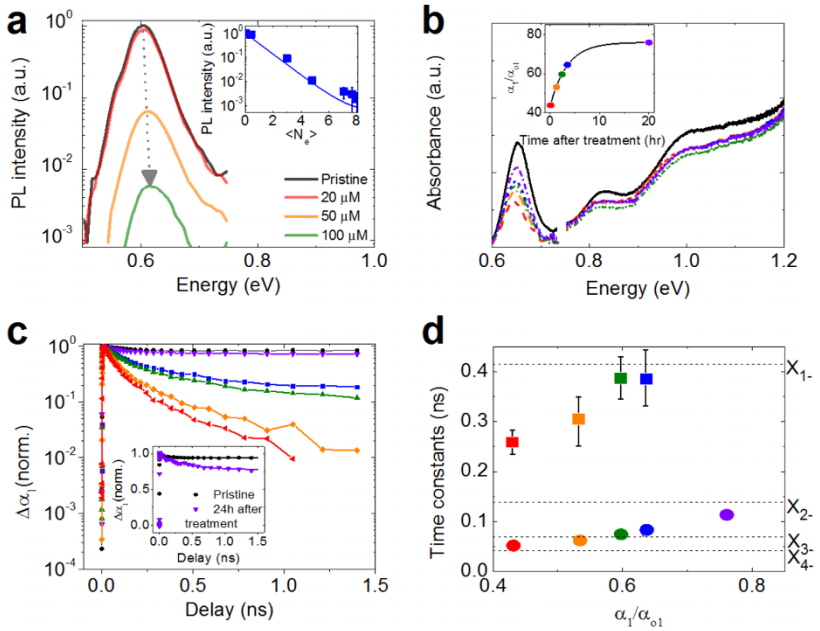

Figure 3 | Spectroscopic signatures of ground-state charging. (a) Cobaltocene-concentration dependent PL quenching of PbSe NCs. Inset: PL intensity (symbols) as a function of the average number of injected electrons derived from $<N_e> = 8|\Delta\alpha_1/\alpha_{o1}|$ along with the calculated PL intensity (line). (b) Absorption spectrum of pristine PbSe NCs (solid black line) along with spectra of treated NCs at different times during absorption recovery (dashed and dashed-dotted lines). Inset: Recovery of 1S band-edge absorption, color-coding is the same as in the main panel. (c) 1S TA dynamics of the sample from (b) during 1S absorption recovery (color coding is the same as in panel b); pump photon energy is 1.55 eV and excitation flux corresponds to N_{ph} = 0.4 absorbed photon per pulse per NC. Inset: Low fluence scans (N_{ph} = 0.1) of the pristine sample (black) and the treated sample following 20 h recovery (violet). (d) Two time constants (symbols, color coding is the same as in panels b and c) of the recovering sample derived from a double exponential fit of the measured TA decay. Horizontal dashed lines represent Auger lifetimes of the exciton in NCs in the presence of different numbers of excess electrons.

be 104(4) ps. Then we treat the sample with cobaltocene to obtain ~55% bleaching of the 1S feature (Fig. 3b), which corresponds to injection of ~4 electrons per NC. The 1S feature gradually recovers with a timescale of approximately 3.4 hours to a final value of about 76% of its original amplitude (inset of Fig. 3b). As the 1S bleach recovers, we observe TA dynamics (Fig. 3c) which also recover, approaching that of the untreated sample (black symbols). To capture the exciton lifetimes in the most heavily and most lightly doped NCs, we apply a two-exponential fit. The results are plotted in Fig. 3d and compared with the Auger lifetimes for X_{1-}, X_{2-}, X_{3-} and X_{4-} (horizontal lines in Fig. 3d), which were calculated using statistical scaling from biexciton lifetime, $\tau_{A,XX}$. The comparison indicates that the shortest time constant measured for the freshly treated sample is close that of X_{4-}, as expected for NCs doped with ~4 electrons. During the 1S bleach recovery, the initial time constant becomes progressively longer due to discharging of the NCs and eventually approaches the value expected for a trion (X_{1-}). The long time constant in the freshly treated sample lies in between the values expected for X_{1-} and X_{2-}, while the sample which has recovered to the steady state shows values of ~360 ps which is close to the lifetime (416 ps) expected for a negative trion (exciton plus one excess electron). In addition to providing additional evidence for charge injection into NCs, these results represent the first direct measurement of charged exciton dynamics in lead chalcogenide NCs.

Stability of doped charges. As mentioned above, the data in the inset of Fig 3b shows that in standard core-only PbSe NCs, the majority of injected charges seem to escape from the NC on the timescale of tens of hours. Shim *et al.* described a similar recovery in *n*-doped CdSe NCs, which was reported to be mediated by trace amounts of air or water, and accompanied by etching of the NCs[5]. This is not likely to be the operative mechanism in our study: our samples are kept rigorously air- and water-free because we have found that even brief exposure of a doped-NC solution to air leads to complete recovery of spectral features within seconds, well before any sign of the spectral blue-shift associated with air-oxidation of the NCs is observed[11]. Moreover, as can be seen in Fig. 3c, recovery of the 1S absorption is accompanied by a similar recovery in the TA dynamics, which show no sign of the type of efficient recombination centers that generally arise during etching or other degradative processes. One might expect that injected electrons in PbSe NCs are instead slowly quenched at electron trap sites at the surface, or perhaps on the ligands themselves. Such a mechanism could be suppressed by growing an outer shell of a wider-gap semiconductor, which is an effective and much more stable passivation method that would effectively reduce formation of surface trap states. To verify this hypothesis, we encapsulated the PbSe core (diameter = 7.3 nm) with a CdSe shell (0.3 nm thick) using a previously reported method (Fig. 4 a, b)[12]. We observe that even very thin CdSe shell can indeed dramatically extend the lifetime of charges in the PbSe core. As illustrated in Fig. 4c, the PbSe/CdSe core/shell samples maintain a nearly complete bleaching of the 1S feature (that is, *ca.* eight electrons per NC) for at least a month at room temperature. This is a record-long lifetime for injected charges in samples doped *via* chemical treatments, to be compared to previously reported lifetimes for CdSe NCs that did not exceed a few days[5].

The effect of doping on conductivity of NC films. Using these core/shell NCs, we investigated the feasibility of using cobaltocene to dope NCs within already-deposited solid films. PbSe/CdSe NC solutions were drop-cast onto quartz substrates and dried under argon atmosphere; no subsequent ligand exchange or removal steps were applied, so the NCs maintained their native oleate passivation. The substrate-bound NCs were then immersed in a 50 mM solution of cobaltocene in acetonitrile for periods varying from 1 hour to 1 day. The absorption spectra of the PbSe/CdSe NC film following exposure to cobaltocene (Fig. 4d) show the bleach of the 1S feature typical of

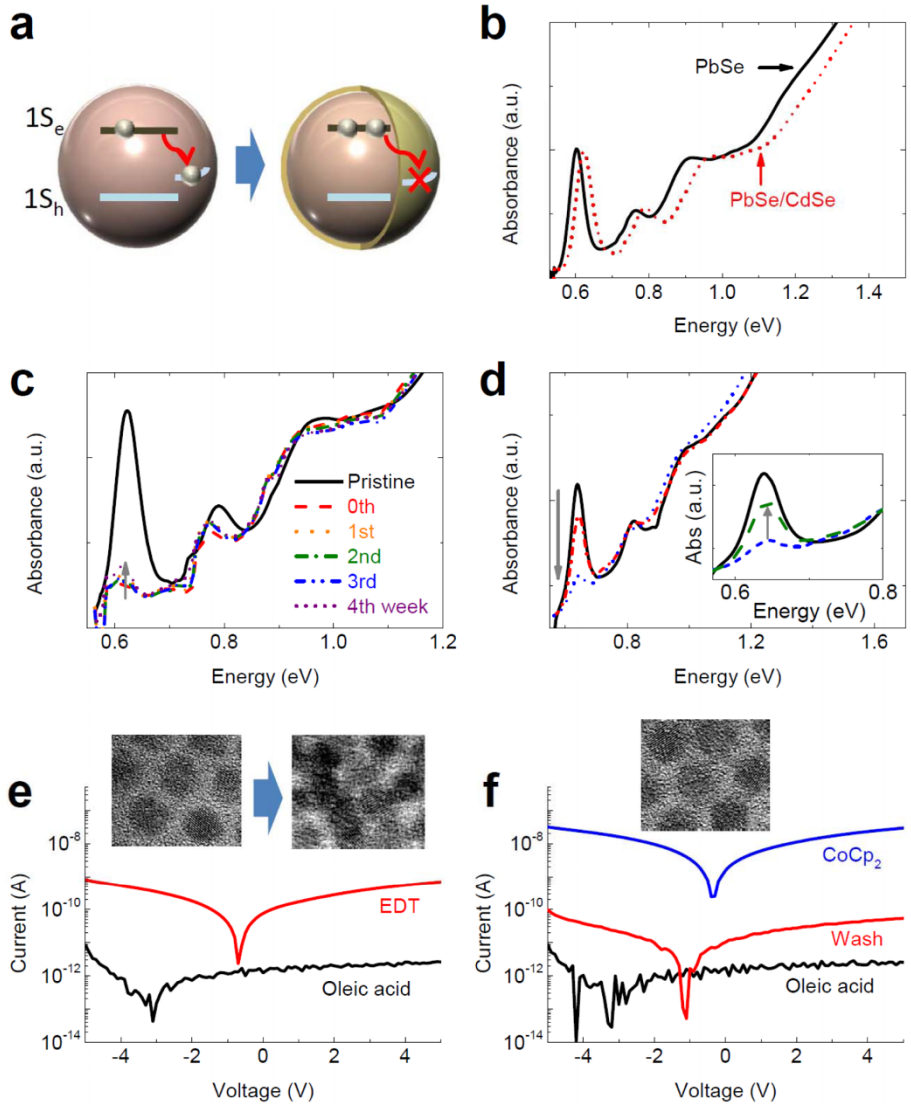

Figure 4 | Cobaltocene doping of PbSe/CdSe NC solution and film samples. (a) Schematic illustration of the effect of a CdSe shell on the stability of doping. (b) Absorption spectra of PbSe NCs before (solid black line) and after shell formation (dotted red line). (c) Absorption spectra of treated PbSe/CdSe NCs during a stability study. (d) Absorption spectra of PbSe/CdSe NC films exposed to cobaltocene solution. Solid black line: pristine film; dashed-dotted red line: 1 hour treatment; dotted blue line: 1 day treatment. Inset: Recovery of bleached absorption spectra of a treated PbSe/CdSe NC film following air exposure. The black and blue lines are from the main panel (same color spectra); the dashed green line corresponds to the sample treated for 1 day with cobaltocene and then exposed to air for 3 min. (e) Conductivity measurements of a pristine PbSe/CdSe NC film treated with EDT (f) The same measurements of NC film treated with cobaltocene. Insets are transmission electron microscopy (TEM) images of pristine (left) and EDT-treated (right) NCs (e), and cobaltocene-treated NCs (f).

doping. This bleach, however, develops much more slowly than in solution samples: after 1 hour of treatment its magnitude is ~30%, and it takes a full day to reach a ~60% bleach. This is consistent with the reduced access of cobaltocene in solution to NCs within the film because of the need to diffusively penetrate the thick film. Nonetheless, these bleach levels indicate injection of up to ~5 electrons per NC on average, demonstrating that with cobaltocene we can produce very high doping levels in both solution and solid-state samples.

Strikingly, these doped PbSe and PbSe/CdSe NC films show a dramatic increase in their conductivity even without ligand exchange. For instance, while traditional EDT-treatment of an undoped PbSe/CdSe NC film can increase conductivity roughly by 2 orders of magnitude (Fig. 4e, 3.0×10^{-10} S cm^{-1} → 7.7×10^{-8} S cm^{-1}), a cobaltocene-doped PbSe/CdSe NC film, without EDT, shows a reversible conductivity enhancement of over 4 orders magnitude (Fig. 4f, 3.2×10^{-10} S cm^{-1} → 3.3×10^{-6} S cm^{-1}). Importantly, TEM images (inset of Fig. 4f), FT-IR (Fig. S3a), and SAXS data (Fig. S3b) confirm that the surface ligand is still oleic acid, and that the interparticle spacing (~1 nm) has not been measurably altered in the conductive cobaltocene-doped NC films. In contrast, both our TEM measurements (inset of Fig. 4e) as well as previous studies[26] have shown that treatment of films with short ligands clearly reduces the average interparticle spacing between NCs (typically to ~4 Å), which is necessary to reduce the barrier for trap-mediated hopping-based transport of charge carriers. This implies that the mechanism of charge transport in doped-NC films is inherently different from that in an EDT-treated film; specifically, we suggest that it occurs instead *via* charge hopping between quantum-confined band-edge states, which are known to have much greater spatial extent than the relatively localized trap states and therefore are somewhat less sensitive to interparticle spacing. Finally, we find that cobaltocene doping is reversible: conductivity of a doped NC film can be decreased nearly to that of the original film

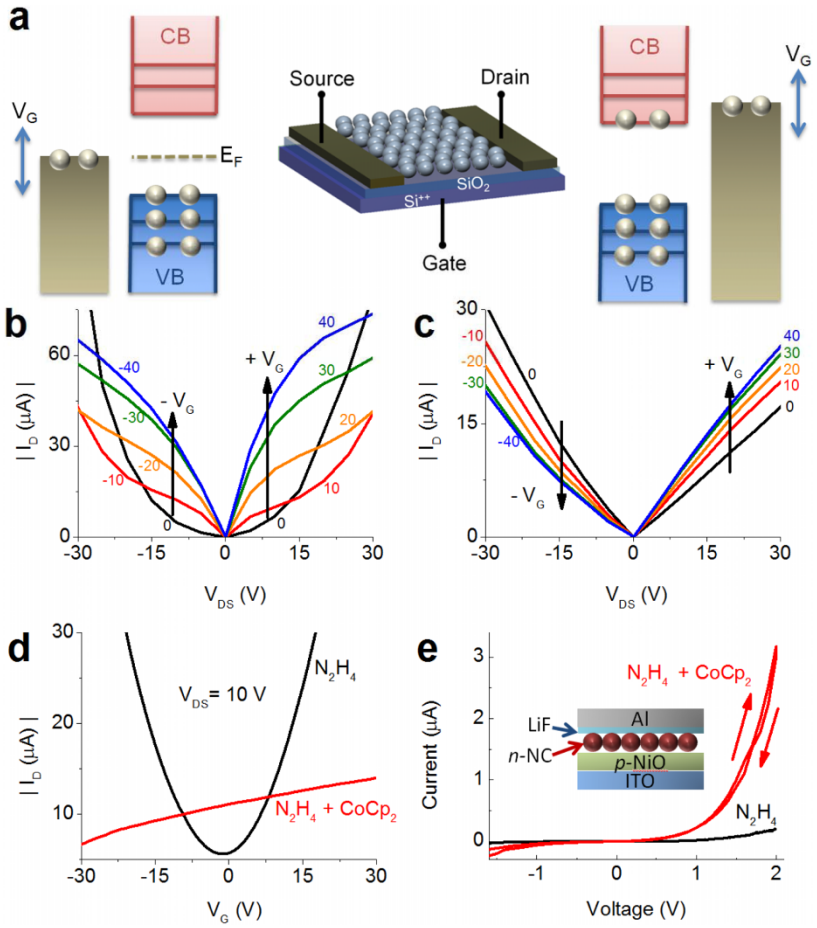

Figure 5 | Field-effect transistor measurements and a *p-n* junction device fabricated from doped NCs. (a) The structure of FETs (middle) along with schematic illustrations of the distributions of electrons across electronic states in intrinsic (*i.e.*, undoped) NCs (left) *vs.* cobaltocene-treated *n*-doped NCs (right). (b) The I_D-*vs.*-V_{DS} characteristics of the PbSe NC-FET treated with hydrazine. (c) The same device after cobaltocene treatment. (d) The I_D-*vs.*-V_{GS} characteristics of the same FETs shown in (a) and (b). (e) The current-voltage (I-V) characteristics of a *p-n* diode for cobaltocene-treated NC films (red) and undoped films, prepared via mild treatment with hydrazine (black). Inset: the structure of the device.

by even quick, gentle washing with pure acetonitrile solvent, further demonstrating that conductivity enhancement is not due to surface trap formation and/or reduction in the inter-particle spacing, both of which would be expected to persist after room-temperature washing.

In order to demonstrate that the enhanced conductivity is a result of the high level of doping in the band-edge states, rather than from any other consequence (e.g., increased carrier mobility) that could result from cobaltocene treatment, we further studied transport in FET devices based on PbSe NC films before and after cobaltocene doping (Fig. 5a). To facilitate these measurements, we have developed a two-step protocol to first reduce interparticle spacing via mild hydrazine treatment and then *n*-dope *via* treatment with cobaltocene. Interestingly, attempts to use EDT treatment as the first step were not successful, likely because EDT introduces surface traps that typically impart *p*-type behavior on PbSe NC films and interfere with cobaltocene doping; thus instead, we used short (~1.5 hr exposure time) treatment with hydrazine.

Heavy treatment with hydrazine has been observed to impart *n*-type doping to PbSe NC films[1]; however, because of the volatility of hydrazine molecules, mild treatment with these species did not produce any doping effect. Specifically the films, that have undergone this type of treatment, show ambipolar and highly symmetric behaviors for positive and negative gate voltages in both I_D-*vs.*-V_{DS} (Fig. 5b) and I_D-*vs.*-V_{GS} (Fig. 5d, black trace) measurements, typical of an intrinsic (*i.e.*, undoped) semiconductor with the Fermi level near the mid-gap position (Fig. 5a; cartoon on the left); I_D is the drain current, and V_{DS} and V_{GS} are the drain-source and the gate-source voltages, respectively.

In sharp contrast, I_D-*vs.*-V_{DS} (Fig. 5c) and I_D-*vs.*-V_{GS} (Fig. 5d, red trace) measurements of a cobaltocene-treated NC film show unipolar behavior and an almost linear dependence of I_D on V_{DS} in the manner expected for an *n*-type conductor with the Fermi level tuned within the conduction band (Fig. 5a; cartoon on the right). Further, in contrast to the pronounced gating effect seen in undoped films (Fig. 5b), changes in V_{GS} only modify the slope of the I_D-V_{DS} dependence, consistent with the situation where the conductance changes due to the V_{GS}–induced variation in the concentration of conduction band electrons. This is also suggested by the I_D-*vs.*-V_{GS} measurements in Fig. 5d (red trace). Importantly, the measurements of both intrinsic and *n*-doped films are highly reproducible over multiple voltage sweeps, and therefore are not associated with any chemical modifications in the NC film during the measurements.

We can use the results of transport studies to derive the doping level of cobaltocene-treated NC films, and then compare the obtained values with those inferred from optical studies. From the FET measurements in Fig. 5d, we calculate an electron mobility (μ_e) of 7.2×10^{-4} cm^2/Vs (see Methods). The fact that this value is much lower than the record mobilities in films comprising NCs re-capped with very short inorganic ligands[27] or films infilled via atomic layer deposition[28] is not surprising. The charge mobilities in NC assemblies are defined by the overlap of wave functions localized on adjacent NCs and are strongly dependent on parameters such as NC-NC

separation and NC-matrix energy band offsets. In our experiments, we did not attempt to improve conductivity by improving mobility, but instead tried to demonstrate the dramatic effect of cobaltocene doping on charge transport which occurs despite fairly low values of μ_e. For a greater contrast, we start with an undoped film comprising widely spaced NCs. As indicated by measurements in Figs. 5b, d without applied gate bias this film is essentially insulating (see estimated charge densities below). However, upon treatment with cobaltocene the film turns into an *n*-type conductor. Specifically, the I_D-*vs*.-V_{DS} dependence measured for zero gate bias shows a nearly Ohmic behavior (Fig. 5c), which allows us to derive Ohmic resistance and then the channel conductivity σ (see Methods). On the basis of data in Fig. 5c, $\sigma = 4.1 \times 10^{-4}$ S cm^{-1} ($V_G = 0$). From this value and the measured mobility, we can calculate a free electron density (n_e) in the NC film, which yields $n_e = \sigma/(e\mu_e) = 3.6 \times 10^{18}$ cm^{-3}. If we assume a random close-packing of NCs in the film, we can estimate the concentration of the NCs in the channel (n_{NC}) from $n_{NC} = 0.64/V_{NC,eff}$, where $V_{NC,eff}$ is the effective NC volume, accounting for the outer ligand shell. From this expression, $n_{NC} = 2.1 \times 10^{18}$ cm^{-3}. Finally, we obtain that the average number of electrons per NC, $\langle N_e \rangle = n_e/n_{NC}$, is 1.7, which is comparable to the values derived from optical studies of samples that have undergone a similar treatment with cobaltocene. Interestingly, the same analysis applied to hydrazine treated films (Fig. 5b, d) indicates that at $V_G = 0$, the density of free charges is only ~0.01 per NC and even under very large gate bias of 40 V it is still below ~0.5 charge per NC.

In the above FET studies, we used core-only PbSe NCs. As we have shown earlier, doping is preserved on much longer timescales in NCs coated with a thin CdSe layer. One concern in the practical application of such structures is a possible detrimental effect of the external shell on charge conductance. However, as we indicated before, due to the large spatial extent of band-edge states, transport via these states is expected to be not significantly hindered by a thin passivating layer. To test the device applicability of core/shell nanostructures, we fabricate *p-n* junction diodes using a NiO *p*-type layer and an *n*-type layer made from PbSe/CdSe NCs treated with the same two-step hydrazine/cobaltocene procedure applied previously to FETs. In Fig 5e, we can see that a *p-n* junction diode of doped NCs indeed shows rectifying behavior in the *I-V* curve (red trace). This is in marked contrast to the response of an undoped hydrazine-treated film (black trace), confirming again that the cobaltocene doping is responsible for the *n*-type behavior and further suggesting that stabilization of dopants with the inorganic passivating shell does not prohibit the use of doped NCs in functional devices.

Discussion

Our experiments showed that we can achieve persistent *n*-type doping in PbSe and PbS NCs via charge-transfer from the relatively mild reducing agent cobaltocene. This method is simple, inexpensive and highly compatible with solution-deposited films of NCs, which can be doped either before or after deposition. Moreover, the *n*-type conductivity is maintained throughout device fabrication of either FETs or simple *p-n* diodes (Fig. 5), even upon ligand removal with hydrazine. The level of doping is also easily controlled by varying the amount of cobaltocence, and can be maintained for months at room temperature if a thin inorganic passivation layer is applied to reduce trap-mediated loss of injected charges.

We confirmed spectroscopically that doped charges, up to eight electrons per NC, populate the $1S_e$ conduction band states, rather than only filling intra-gap surface-related electron traps. This is clearly distinct from previous reports on doping of NC surface-states, particularly in the context of NC-based photovoltaics. Specifically, the wavefunctions of band-edge states exhibit much larger spatial extent than those of surface trap states, yielding much greater overlap, from NC to NC, that can reduce the dependence of conductivity on inter-NC spacing. This is demonstrated most clearly in Fig. 4f, which shows that the doped charges are mobile even when the NCs are separated by their fairly long, native oleate ligands. Further, this allows greater flexibility in the choice of surface treatments to NC films to enhance surface-trap passivation and lower carrier recombination losses. Additionally, while conductivity through intra-gap trap-states leads to lower potential in photovoltaics (as carriers relax into intra-gap states well below the nominal NC conduction band-edge to be transported[9]), the ability to transport charges through band edge states eliminates this specific cause of reduced voltage. Finally, transport through band edge states allows one to fully tune, through NC size, the band alignment between the NC absorbing layer and other device layers in a photovoltaic device (*e.g.*, collecting electrodes) to further maximize the photovoltage. Thus, these results constitute the first example of a potential generalizable method for solution-based doping that can be of unique value to the ongoing development of NC-based photovoltaics. The use of this novel doping technique should also facilitate studies of the effect of persistent charges on the fundamental photophysical and charge-transport properties of colloidal nanostructures.

Methods

Cobaltocene treatment of NC solution and film samples. All syntheses and manipulations were carried out under dry argon using standard Schlenk-line and glove-box techniques. PbSe NCs, PbSe/CdSe, and PbS NCs were prepared by previously reported methods[12,29,30]. Typically, a dispersion of NCs in toluene (0.5 ml, ~1.5 μM) was mixed with an equal amount of a solution of cobaltocene in toluene (~5 mM – 20 μM). For the FT-IR measurements (as shown in Fig 2d), mixed solutions of NCs (~1.5 μM) and cobaltocene (~25 mM) were drop-cast onto a zinc selenide window and dried under argon atmosphere. For the cobaltocene treatment of PbSe/CdSe NC films (as shown in Fig. 4d), NC solutions were drop-cast onto quartz substrates and dried under argon atmosphere. The sample was then immersed in a solution of cobaltocene in acetonitrile (5 mM) for a period of time ranging from one hour to one day (see main text). Then, it was transferred into a customized sealed quartz cell to prevent air exposure. We observed that even brief exposure to air resulted in a quick bleach recovery indicating the loss of doping (inset of Fig. 4d).

Visible-near-infrared absorption, PL, and Fourier transformed infrared (FT-IR) spectroscopies. Absorption spectra were taken in transmission mode on a Perkin-Elmer Lambda 1050 UV/vis/NIR spectrophotometer at 2 nm spectral bandwidth. The absorption spectra were measured for NC films on quartz, and NC dispersions in standard air-free quartz cuvettes with airtight seals. The concentration of NCs solutions were calculated using the molar extinction coefficients ε (at 400 nm) = $0.0277d^3$ cm^{-1}μM^{-1} and $0.0233d^3$ cm^{-1}μM^{-1} for PbSe and PbS NCs, respectively, where d is the NC diameter in nm[31,32]. The steady-state PL spectra were collected through a monochromator and detected by a liquid N_2-cooled InSb detector using an 808 nm diode laser for excitation. FT-IR spectra were taken in transmission mode on a Thermo-Fisher 6700 FT-IR spectrometer at a spectral resolution of 4 cm^{-1}. Spectra of NC films were taken in a demountable liquid cell with zinc selenide windows and 0.1 mm Teflon spacers (Pike technologies).

TA spectroscopy. The TA setup used here has been discussed in detail previously[25]. Briefly, samples are excited with ~100 fs (FWHM), 1.55 eV pulses from a 1 kHz Ti–sapphire amplifier. Pump-induced changes in the absorption spectra are then associated with state-filling of the 1S transition. The size of this bleach is directly proportional to the number of electrons in the 1S state and monitoring this state as a function of time reveals carrier dynamics.

Sample preparation for conductivity measurements. For conductivity measurements, NC films were spin-coated from a solution of NCs in hexane at 2500 rpm onto clean glass substrates with interdigitated source and drain electrodes (30 nm thick Au) spaced 50 μm apart. They were immersed in either 1,2-ethanedithiol solution in acetonitrile (~1% w/w) for 30 sec, or cobaltocene in acetonitrile solution (5 mM) overnight.

FET measurements. The $m = 3$ periods of 30 nm thick Au interdigitated electrodes (length $L = 50$ μm and spacing $w = 10$ mm) were thermally deposited using a shadow mask on doped Si wafers with a thermally grown 250 nm thick layer of SiO_2. A PbSe NC (diameter $d = 6.9$ nm) film was deposited by casting a NC layer onto the surface of acetonitrile and then transferring it to the electrode-patterned substrate by the method described in a previous report[33]. After deposition of each layer, the whole substrate was immersed in 1 M hydrazine in acetonitrile for 30 min. The layer transfer and hydrazine treatment were then repeated three times to produce crack-free films (total thickness h of ca. 50 nm), which were subsequently immersed in 5 mM cobaltocene in toluene for 20 min.

Device characterization was performed using a semiconductor analyzer (B1500A, Agilent). The mobilities μ were calculated using the gradual channel approximation

equation in the linear regime, $\frac{\partial I_D}{\partial V_G} = \frac{WCV_{DS}}{L}\mu$, where $C = 13.8$ nF/cm^2 is the capacitance per unit area of the gate oxide, and W and L are the channel width and length, respectively; in the case of interdigitated electrodes, $W = (2\ m - 1)w$, which yields $W = 50$ mm for our structures.

The I_D-*vs*.-V_{DS} characteristics of cobaltocene doped films are nearly Ohmic, which allows us to derive from them the usual Ohmic resistance, $R = dV_{DS}/dI_D$, and subsequently, using the geometrical parameters of our FETs, the conductivity $\sigma = L\ [Rhw(2\ m\ -\ 1)]^{-1}$.

Fabrication of *p-n* diodes. *p*-NiO (~10 nm thick) was deposited onto an ITO substrate by spin coating 100 mM nickel acetate in 2-ethoxyethanol at 4000 rpm, and annealed at 130°C for 5 min, 250°C for 5 min, and 350°C for 30 min, sequentially. PbSe/CdSe NC (core = 6.6 nm and shell = 0.2 nm thick) layer was deposited on top of NiO layer by the same way described above. The layer transfer and hydrazine treatment (> two hours for each layer) were then repeated six times to produce crack-free films (~50–70 nm thick), which were subsequently immersed in 5 mM cobaltocene in toluene overnight. Finally, lithium fluoride (5 nm thick) and aluminum electrode (80 nm thick) were thermally deposited using a shadow mask. Device measurements were carried out with Keithley 2400 SourceMeter.

1. Talapin, D. V. & Murray, C. B. PbSe Nanocrystal Solids for n- and p-Channel Thin Film Field-Effect Transistors. *Science* **310**, 86–89 (2005).
2. Semonin, O. E., Luther, J. M., Choi, S., Chen, H.-Y., Gao, J., Nozik, A. J. & Beard, M. C. Peak External Photocurrent Quantum Efficiency Exceeding 100% via MEG in a Quantum Dot Solar Cell. *Science* **334**, 1530–1533 (2011).
3. Sun, L., Choi, J. J., Stachnik, D., Bartnik, A. C., Hyun, B.-R., Malliaras, G. G., Hanrath, T. & Wise, F. W. Bright infrared quantum-dot light-emitting diodes through inter-dot spacing control. *Nat. Nanotech.* **7**, 369–373 (2012).
4. Mocatta, D., Cohen, G., Schattner, J., Millo, O., Rabani, E. & Banin, U. Heavily Doped Semiconductor Nanocrystal Quantum Dots. *Science* **332**, 77–81 (2011).
5. Shim, M. & Guyot-Sionnest, P. n-type colloidal semiconductor nanocrystals. *Nature* **407**, 981–983 (2000).
6. Engel, J. H., Surendranath, Y. & Alivisatos, A. P. Controlled Chemical Doping of Semiconductor Nanocrystals Using Redox Buffers. *J. Am. Chem. Soc.* **134**, 13200–13203 (2012).
7. Wehrenberg, B. L. & Guyot-Sionnest, P. Electron and Hole Injection in PbSe Quantum Dot Films. *J. Am. Chem. Soc.* **125**, 7806–7807 (2003).
8. Klem, E. J. D., Shukla, H., Hinds, S., MacNeil, D. D., Levina, L. & Sargent, E. H. Impact of dithiol treatment and air annealing on the conductivity, mobility, and hole density in PbS colloidal quantum dot solids. *Applied Physics Letters* **92**, 212105 (2008).
9. Nagpal, P. & Klimov, V. I. Role of mid-gap states in charge transport and photoconductivity in semiconductor nanocrystal films. *Nat. Commun.* **2**, 486 (2011).
10. Geyer, S. M., Allen, P. M., Chang, L.-Y., Wong, C. R., Osedach, T. P., Zhao, N., Bulovic, V. & Bawendi, M. G. Control of the Carrier Type in InAs Nanocrystal Films by Predeposition Incorporation of Cd. *ACS Nano* **4**, 7373–7378 (2010).
11. Sykora, M., Koposov, A. Y., McGuire, J. A., Schulze, R. K., Tretiak, O., Pietryga, J. M. & Klimov, V. I. Effect of Air Exposure on Surface Properties, Electronic Structure, and Carrier Relaxation in PbSe Nanocrystals. *ACS Nano* **4**, 2021–2034 (2010).
12. Pietryga, J. M., Werder, D. J., Williams, D. J., Casson, J. L., Schaller, R. D., Klimov, V. I. & Hollingsworth, J. A. Utilizing the Lability of Lead Selenide to Produce Heterostructured Nanocrystals with Bright, Stable Infrared Emission. *J. Am. Chem. Soc.* **130**, 4879–4885 (2008).
13. Hanrath, T., Veldman, D., Choi, J. J., Christova, C. G., Wienk, M. M. & Janssen, R. A. J. PbSe Nanocrystal Network Formation during Pyridine Ligand Displacement. *ACS Appl. Mater. Interfaces* **1**, 244–250 (2009).
14. Connelly, N. G. & Geiger, W. E. Chemical Redox Agents for Organometallic Chemistry. *Chemical Reviews* **96**, 877–910 (1996).
15. Hyun, B.-R., Zhong, Y.-W., Bartnik, A. C., Sun, L., Abruña, H. D., Wise, F. W., Goodreau, J. D., Matthews, J. R., Leslie, T. M. & Borrelli, N. F. Electron Injection from Colloidal PbS Quantum Dots into Titanium Dioxide Nanoparticles. *ACS Nano* **2**, 2206–2212 (2008).
16. Jasieniak, J., Califano, M. & Watkins, S. E. Size-Dependent Valence and Conduction Band-Edge Energies of Semiconductor Nanocrystals. *ACS Nano* **5**, 5888–5902 (2011).
17. Kang, I. & Wise, F. W. Electronic structure and optical properties of PbS and PbSe quantum dots. *J. Opt. Soc. Am. B* **14**, 1632–1646 (1997).
18. Klimov, V. I. Spectral and Dynamical Properties of Multiexcitons in Semiconductor Nanocrystals. *Annu. Rev. Phys. Chem.* **58**, 635–673 (2007).
19. Voznyy, O., Zhitomirsky, D., Stadler, P., Ning, Z., Hoogland, S. & Sargent, E. H. A Charge-Orbital Balance Picture of Doping in Colloidal Quantum Dot Solids. *ACS Nano*, (2012).
20. Goupalov, S. V. Selection rules for optical transitions in PbSe nanocrystal quantum dots: Drastic effect of structure inversion asymmetry. *Phy. Rev. B* **79**, 233305 (2009).
21. McGuire, J. A., Joo, J., Pietryga, J. M., Schaller, R. D. & Klimov, V. I. New Aspects of Carrier Multiplication in Semiconductor Nanocrystals. *Acc. Chem. Res.* **41**, 1810–1819 (2008).
22. McGuire, J. A., Sykora, M., Robel, I. n., Padilha, L. A., Joo, J., Pietryga, J. M. & Klimov, V. I. Spectroscopic Signatures of Photocharging due to Hot-Carrier Transfer in Solutions of Semiconductor Nanocrystals under Low-Intensity Ultraviolet Excitation. *ACS Nano* **4**, 6087–6097 (2010).
23. Wehrenberg, B. L., Wang, C. & Guyot-Sionnest, P. Interband and Intraband Optical Studies of PbSe Colloidal Quantum Dots. *J. Phy. Chem. B* **106**, 10634–10640 (2002).
24. Klimov, V. I., McGuire, J. A., Schaller, R. D. & Rupasov, V. I. Scaling of multiexciton lifetimes in semiconductor nanocrystals. *Phy. Rev. B* **77**, 195324 (2008).
25. Stewart, J. T., Padilha, L. A., Qazilbash, M. M., Pietryga, J. M., Midgett, A. G., Luther, J. M., Beard, M. C., Nozik, A. J. & Klimov, V. I. Comparison of Carrier Multiplication Yields in PbS and PbSe Nanocrystals: The Role of Competing Energy-Loss Processes. *Nano Lett.* **12**, 622–628 (2011).
26. Talapin, D. V., Lee, J.-S., Kovalenko, M. V. & Shevchenko, E. V. Prospects of Colloidal Nanocrystals for Electronic and Optoelectronic Applications. *Chemical Reviews* **110**, 389–458 (2009).
27. Oh, S. J., Berry, N. E., Choi, J.-H., Gaulding, E. A., Paik, T., Hong, S.-H., Murray, C. B. & Kagan, C. R. Stoichiometric Control of Lead Chalcogenide Nanocrystal Solids to Enhance Their Electronic and Optoelectronic Device Performance. *ACS Nano* **7**, 2413–2421 (2013).
28. Liu, Y., Tolentino, J., Gibbs, M., Ihly, R., Perkins, C. L., Liu, Y., Crawford, N., Hemminger, J. C. & Law, M. PbSe Quantum Dot Field-Effect Transistors with Air-Stable Electron Mobilities above 7 cm2 V–1 s–1. *Nano Letters* **13**, 1578–1587 (2013).
29. Hines, M. A. & Scholes, G. D. Colloidal PbS Nanocrystals with Size-Tunable Near-Infrared Emission: Observation of Post-Synthesis Self-Narrowing of the Particle Size Distribution. *Adv. Mater.* **15**, 1844–1849 (2003).
30. Joo, J., Pietryga, J. M., McGuire, J. A., Jeon, S.-H., Williams, D. J., Wang, H.-L. & Klimov, V. I. A Reduction Pathway in the Synthesis of PbSe Nanocrystal Quantum Dots. *J. Am. Chem. Soc.* **131**, 10620–10628 (2009).
31. Moreels, I., Lambert, K., De Muynck, D., Vanhaecke, F., Poelman, D., Martins, J. C., Allan, G. & Hens, Z. Composition and Size-Dependent Extinction Coefficient of Colloidal PbSe Quantum Dots. *Chem. Mater.* **19**, 6101–6106 (2007).
32. Moreels, I., Lambert, K., Smeets, D., De Muynck, D., Nollet, T., Martins, J. C., Vanhaecke, F., Vantomme, A., Delerue, C., Allan, G. & Hens, Z. Size-Dependent Optical Properties of Colloidal PbS Quantum Dots. *ACS Nano* **3**, 3023–3030 (2009).
33. Koh, W.-k., Saudari, S. R., Fafarman, A. T., Kagan, C. R. & Murray, C. B. Thiocyanate-Capped PbS Nanocubes: Ambipolar Transport Enables Quantum Dot Based Circuits on a Flexible Substrate. *Nano Lett.* **11**, 4764–4767 (2011).

Acknowledgements

W.-k. K., A.Y.K., I.R., J.M.P. and V.I.K. acknowledge support of the Center for Advanced Solar Photophysics (CASP), an Energy Frontier Research Center funded by the U.S. Department of Energy, Office of Science, Office of Basic Energy Sciences (OBES). J.T.S is a CASP member supported by LANL Director's Postdoctoral Fellowship. The authors are grateful to Darrick J. Williams for conducting small-angle X-ray scattering measurements, Qianglu Lin for providing PbSe/CdSe core/shell NC samples, Hue Nguyen for help with LabView programming, and Youngil Park for assistance in FT-IR measurements.

Author contributions

V.I.K., A.Y.K. and W.-k. K. conceived the study. W.-k. K. and A.Y.K. investigated cobaltocene doping of the NCs under the guidance of J.M.P. and V.I.K. J.T.S. and I.R. performed TA measurements. W.–k. K. fabricated and measured device structures with assistance of B.N.P. All authors analyzed and interpreted the data. V.I.K. and W.-k. K. prepared the manuscript with the assistance of J.T.S. and J.M.P. and inputs from other co-authors.

Additional information

Supplementary information accompanies this paper at http://www.nature.com/scientificreports

Competing financial interests: The authors declare no competing financial interests.

How to cite this article: Koh, W.-K. *et al.* Heavily doped *n*-type PbSe and PbS nanocrystals using ground-state charge transfer from cobaltocene. *Sci. Rep.* **3**, 2004; DOI:10.1038/srep02004 (2013).